Nuclear Instruments and Methods in Physics Research B 321 (2014) 54–58

Contents lists available at ScienceDirect

Nuclear Instruments and Methods in Physics Research B

journal homepage: www.elsevier.com/locate/nimb

Residual defects in low-dose arsenic-implanted silicon after high-temperature annealing

Akihiko Sagara [a,*], Miori Hiraiwa [a], Akira Uedono [b], Nagayasu Oshima [c], Ryoichi Suzuki [c], Satoshi Shibata [a]

[a] Panasonic Corporation, 3-1-1 Yagumo-nakamachi, Moriguchi, Osaka 570-8501, Japan
[b] University of Tsukuba, 1-1-1 Tennôdai, Tsukuba, Ibaraki 305-8573, Japan
[c] National Institute of Advanced Industrial Science and Technology, 1-1-1 Umezono, Tsukuba, Ibaraki 305-8563, Japan

ARTICLE INFO

Article history:
Received 17 October 2013
Received in revised form 25 December 2013

Keywords:
Residual damage
Ion-implantation
Arsenic
Silicon
Cathodoluminescence
Positron annihilation spectroscopy

ABSTRACT

We investigated the residual defects in low-dose (10^{13} cm^{-2}) arsenic implanted Si after high-temperature (1100 °C) annealing. The presence of residual damage was successfully revealed after using a rapid thermal process for heat treatment. This damage was identified as vacancy-type defects distributed near the surface, such as tetravacancies or pentavacancies. When O_2 gas was introduced to the annealing chamber, vacancy-type defects were transformed into divacancy and carbon–oxygen complex. They were confirmed to be created by a non-equilibrium reaction during the rapid cooling-down step in the annealing sequence.

1. Introduction

Impurity implantation is an essential process for manufacturing silicon (Si) devices. Since the accelerated ions introduce lattice damage during implantation, subsequent annealing must be applied to heal the damage as well as to activate the impurities. If the implant damage is not eliminated, it may cause degradation of the device's performance. Therefore, residual damage that persists after annealing is a matter of growing concern in the Si semiconductor industry [1].

One example is end-of-range (EOR) defects. If the implant dose is higher than the critical dose of amorphization (10^{14}–10^{16} cm^{-2}), dislocation loops can be created even after annealing beyond the amorphous/crystalline interface. These defects have been evaluated by transmission electron microscopy (TEM) [2,3] and Rutherford backscattering spectrometry (RBS) since 1960's [4,5]. They have been confirmed to lead to the fatal problem of junction leakage and/or transient enhanced diffusion (TED) [6,7]. In contrast, even under low-dose implant conditions that are below the critical dose (<10^{13} cm^{-2}), point defects are known to remain when the annealing temperature is relatively low (<700 °C). These defects have been investigated using optical and electrical characterization methods such as electron spin resonance (ESR) [8,9], infrared absorption spectroscopy (IR) [10,11], photoluminescence (PL) [12,13] and deep transient level spectroscopy (DLTS) [14,15]. For the last 50 years, numerous studies have been carried out on these defects and their annealing behavior under low-dose implant conditions. However, there are few reports on defects that develop after applying high-temperature (>1000 °C) annealing: they have not been directly characterized in low-dose implanted and high-temperature annealed Si [16,17]. The conventional view is that no damage remains under these conditions, but that if it does exist, it has minimal influence on device performance. Little attention has thus been paid to defects that might remain after low-dose implantation processes.

In a previous study, we showed the presence of residual damage in low-dose (10^{13} cm^{-2}) arsenic (As) implanted Si after high-temperature (>1000 °C) annealing when using rapid thermal processes for heat treatment [18]. The characterization technique we used was a cathodoluminescence (CL) method [19,20]. Applying the CL technique to Si materials has been restricted because of its low luminescence efficiency. However, we have shown this technique, when used to compare luminescent intensity, to be an efficient tool for characterizing a various kinds of defects and/or crystal disorders. CL analysis clearly revealed that non-radiative decay centers are present in the crystal [18].

* Corresponding author. Address: Device Solutions Center, R&D division, Panasonic Corporation, 3-1-1 Yagumo-nakamachi, Moriguchi, Osaka 570-8501, Japan. Tel.: +81 6 6906 4916; fax: +81 6906 3407.
E-mail address: sagara.akihiko@jp.panasonic.com (A. Sagara).

0168-583X/$ - see front matter © 2014 Elsevier B.V. All rights reserved.
http://dx.doi.org/10.1016/j.nimb.2013.12.026

We undertook this study to clarify the details of the damage. We prepared low-dose (10^{13} cm^{-2}) As implanted Si and subjected it to rapid thermal annealing (RTA) at a high temperature (1100 °C). We also introduced oxygen (O_2) to the annealing chamber in addition to nitrogen (N_2). We evaluated the residual damage using positron annihilation spectroscopy (PAS) in addition to the CL method. The defects and their evolution during annealing were investigated by comparison with carrier properties obtained by sheet resistance measurements.

2. Experimental

Fig. 1 shows the process of making of the samples used in this investigation. The base material was a p-type Cz-Si wafer with (100) orientation. After a 10 nm-thick thermal oxide layer was grown, As^+ ions were implanted at normal incidence angle through the oxide layer at 150 keV to a dose of 1.0×10^{13} cm^{-2}. The samples were annealed at a top temperature of 1100 °C for 50 s using a hot-wall type RTA system. The heating rate and cooling rate were set at 40 and 80 °C/s respectively. Nitrogen (N_2) and oxygen (O_2) mixed gas was introduced to the annealing chamber at various O_2 concentrations (0%, 5%, 10%, 20% and 30%). An oxide-layer-only grown sample was prepared as reference, and an as-implanted sample was also prepared for comparison.

For cathodoluminescence (CL) measurements, a Hitachi S-4300SE scanning electron microscope (SEM) with a Schottky emission-type gun was used as the excitation source. The acceleration voltage of the electron beam was 15 kV. The emitted luminescence was collected using an ellipsoidal mirror and optical fiber, and analyzed using a Jobin Yvon HR-320 single monochromator equipped with an InGaAs multichannel detector. All CL measurements were performed at 30 K. The details of the CL measurement system are described elsewhere [21,22].

The sheet resistance was measured using a Frontier Semiconductor RsL300, a non-contact photo-voltage based sheet resistance and leakage current mapping tool [23]. The wavelength and Rs frequency of the modulated LED were 700 nm and 100 kHz. The 1000 iterated measurements of each point improved repeatability by up to 0.08% [23].

Before positron annihilation spectroscopy (PAS) analysis, the oxide layers were removed with hydrofluoric (HF) acid. The Doppler broadening spectra of the positron annihilation radiation were measured with a Ge detector as a function of the incident positron energy. The low-momentum part of the spectra was characterized using the S parameter, which was defined as the number of annihilation events over the energy range of 511 keV ± ΔE (where ΔE = 0.76 keV). This S parameter is an index of the amount and size of vacancy-type defects [24]. The relationship between S and E was analyzed using VEPFIT, a computer program developed by van Veen et al. [25]. The depth distributions of the S parameter were obtained by fitting the S–E curve. The W parameter, defined as the number of annihilation events in the range of 3.4 keV $\leqslant \Delta E \leqslant$ 6.8 keV, was also obtained to examine the annihilation characteristics in detail. The lifetime spectra of positrons were measured using a pulsed monoenergetic positron beam [26]. The incident positron energy was fixed at 1 keV. The positron lifetime and its intensity of the ith component, τ_i and I_i, are given by analyzing the lifetime spectra using a computer program called RESOLUTION [27]. The details of the PAS measurement system are described elsewhere [28,29].

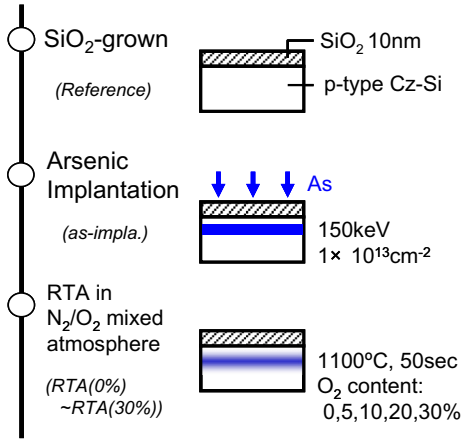

Fig. 1. Fabrication of the samples used in this investigation.

3. Results and discussion

Fig. 2 shows the CL spectra of all the samples. Two emission lines, labeled TO and TO + O^{Γ}, can be observed in the spectrum of the reference sample. These lines are typical band-to-band transitions followed by the emission of transverse optical (TO) phonons and optical phonons at $k = 0$ (O^{Γ}) [30]. No peaks can be seen other than the TO and TO + O^{Γ}-lines. It can thus be concluded that the defect density is low just after the oxide layer has grown. In contrast, the intensity of the TO-line is reduced after As implantation. A W-line, C-line and broad band in the long-wavelength region are detected in the spectrum of the as-implanted sample. The W-line emission is considered to originate from Si self-interstitial clusters [30–33]. The C-line is well recognized as the emission from the interstitial carbon and interstitial oxygen (C_i–O_i) complex [30,34–36]. The origin of the broad band is not clear. It might be due to certain point defects or their complexes being broadened by an inhomogeneous disorder in the lattice. These defect-related lines reflect the development of implant damage caused by the impact of accelerated As ions. When this implanted sample was

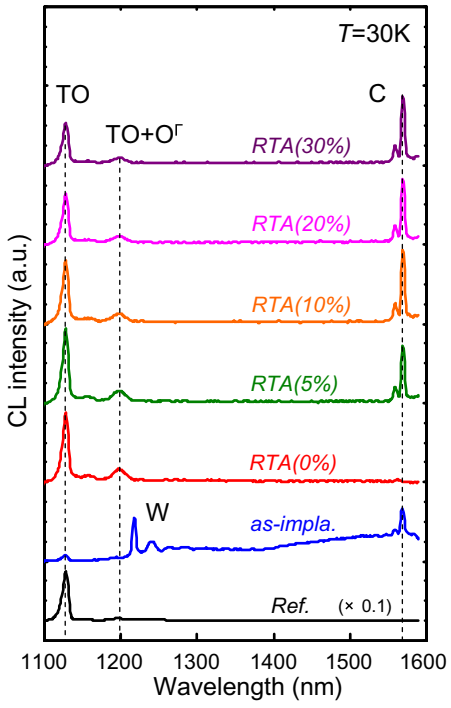

Fig. 2. CL spectra of reference, as-implanted and RTA-applied samples with various proportion of O_2 concentration in the annealing atmosphere (0%, 5%, 10%, 20% and 30%).

annealed using the RTA system at a high temperature of 1100 °C in a 100% N_2 atmosphere (O_2: 0%), all the defect-related lines disappeared and the TO-line reappeared. This means that the implant damage had been annealed out and the crystallinity had been partially regained. However, the TO-line intensity of the RTA-applied sample is one order lower than that of the reference sample. This suggests that the TO-line emission had been suppressed by non-radiative decay centers, i.e., some kind of defect and/or crystal disorder. This provides strong evidence of the presence of residual damage.

When O_2 gas was introduced to the reactor chamber during the RTA process, the C-line reappeared. The C_i–O_i complex, which is the origin of the C-line emission as mentioned above, has been reported to vanish at relatively low temperatures of up to 600 °C [30,36]. Nevertheless, it remains after annealing at 1100 °C. This result can be explained by assuming that the C_i–O_i complex is created by a non-equilibrium reaction that takes place during the extremely rapid cooling step (80 °C/s) in the annealing sequence. Fig. 3 shows the C/TO relative intensity, which is defined as C-line intensity divided by TO-line intensity, with various proportions of O_2 content in the annealing atmosphere. The C/TO relative intensity clearly increases with O_2 content, suggesting that the amount of C_i–O_i complex increased with rising O_2 concentration. This implies that the oxygen in the annealing chamber penetrated the oxide layer and combined with the carbon in the crystal. The sheet resistance variation of RTA-applied samples is also shown in the same Figure. The sheet resistance fell with increasing O_2 content, showing an opposite pattern to C/TO relative intensity. This confirms the presence of damage after RTA, even in a 100% N_2 atmosphere (O_2: 0%), as mentioned above. It suggests that this defect forms the deep level in the band gap and act as a non-radiative decay center. Its capture cross-section should be larger than that of the defects that remain after RTA in an O_2-containing atmosphere [37,38]. It can be concluded that residual damage certainly exists, even after high-temperature annealing, but that it is transformed into other types of defects, such as C_i–O_i complex, on combination with oxygen in the annealing atmosphere.

To clarify the defect species and their locations, all samples were evaluated using the PAS technique. The *S* parameters as a function of incident positron energy *E* are shown in Fig. 4. The *S* value of as-implanted sample was higher than that of reference sample and was distributed in a higher range of positron energy. This is likely to represent implant damage created by accelerated ions. Although the *S* value decreased after annealing, it was still higher

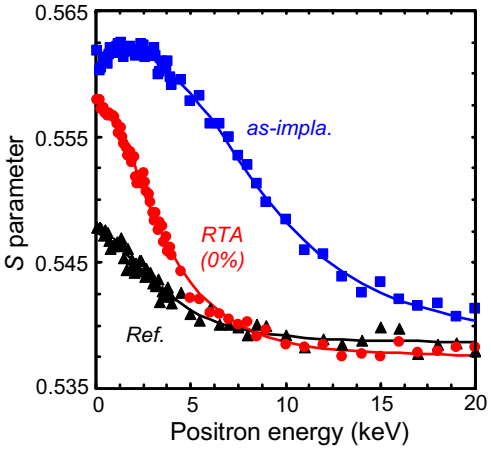

Fig. 4. *S* parameters as a function of incident positron energy *E* for reference, as-implanted and RTA-applied sample. The solid curves are fits to the experimental data.

than that of the reference sample. This means that a proportion of residual damage, which we understand from the CL results to be non-radiative decay centers, was identified as vacancy-type defects. The solid curves shown in Fig. 4 are fitted to the experimental data. The derived depth distributions of the *S* values are shown in Fig. 5. The As depth profiles obtained using secondary ion mass spectrometry (SIMS) are shown in the same Figure. The distribution of *S* values in the as-implanted sample is similar to the As depth profile. In contrast, the *S* value of the RTA-applied samples was distributed in the surface region up to a few tens of nanometers. This result indicates that vacancy-type defects were present near the surface region, which is shallower than the As-implanted region.

Fig. 6 shows the *S*–*E* curves of the reference and RTA-applied samples with various concentrations of O_2 in the annealing atmosphere. The mean implantation depth of positrons in Si crystal are calculated and described on the upper *x*-axis in the same Figure [28]. The *S* values of the RTA-applied samples decreased with increasing O_2 concentration in the annealing atmosphere. The *W* parameters were obtained, and the correlation between the *S* parameters are plotted in Fig. 7. It can be seen that the *W* values increased with falling *S* values. However, the *S*–*W* plot did not

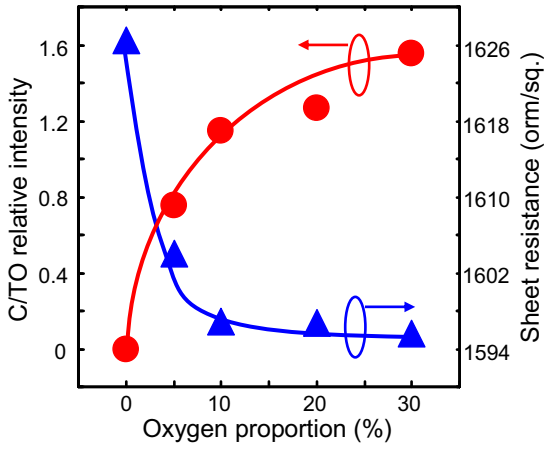

Fig. 3. C/TO relative intensity and sheet resistance variation of RTA-applied samples with various proportion of O_2 concentration in the annealing atmosphere (0%, 5%, 10%, 20% and 30%).

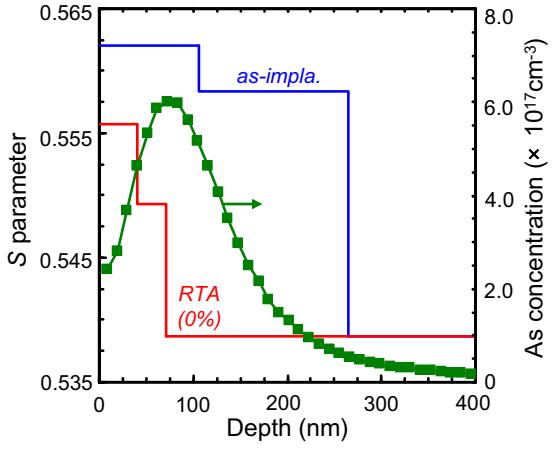

Fig. 5. The depth distribution of *S* parameters of as-implanted and RTA-applied sample. The results were fitted and calculated from *S*–*E* relationship shown in Fig. 4. The depth profiles of As concentration measured using SIMS are also shown in comparison.

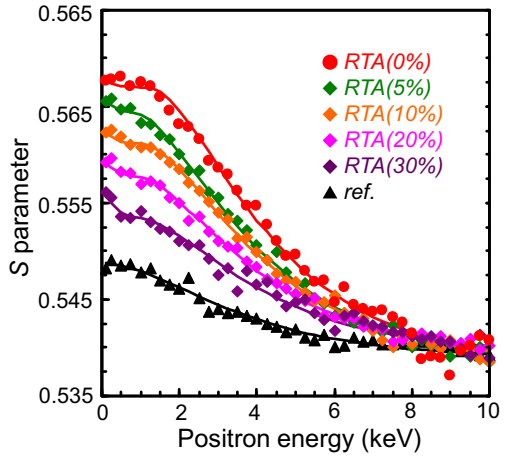

Fig. 6. *S* parameters as a function of incident positron energy *E* for RTA-applied samples with various proportion of O_2 concentration in the annealing atmosphere (0%, 5%, 10%, 20% and 30%). The plot of reference sample is also shown in comparison. The solid curves are fits to the experimental data.

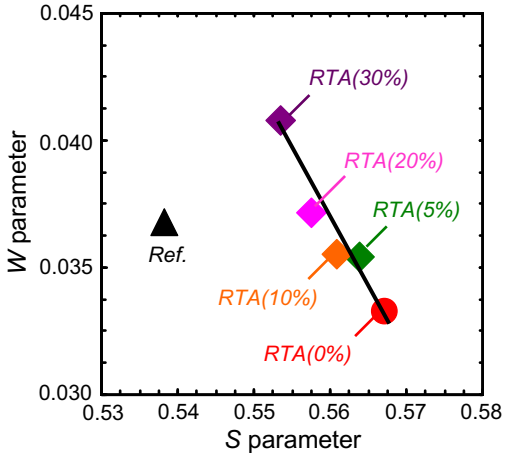

Fig. 7. *S*–*W* relationships for RTA-applied samples with various proportion of O_2 concentration in the annealing atmosphere (0%, 5%, 10%, 20% and 30%). The plot of reference sample is also shown in comparison.

approach the value of the reference sample. This indicates that the residual defects in the RTA-applied sample in a 100% N_2 atmosphere (O_2: 0%) did not simply vanish, but instead created new defects with increasing O_2 content. Table 1 lists the lifetimes of positrons and their intensities in the RTA-applied samples in atmospheres with different O_2 concentrations. The lifetime of positron in the RTA-applied sample in a 100% N_2 atmosphere (O_2: 0%) was analyzed, assuming a single annihilation mode. Its value was 359 ± 1 ps. In the light of previous results, this defect is likely to be a tetravacancy (V_4) or pentavacancy (V_5) [39–42]. In contrast, the lifetime spectra for the RTA-applied sample in an O_2-containing atmosphere (O_2: 30%) was decomposed into two components. The average values of τ_1 and τ_2 were 198 ± 1 and 320 ± 1 ps (I_2 = 36%), respectively. The average τ_1 was close to the lifetime of positrons trapped by a divacancy (V_2) [39–42]. The value of τ_2 was smaller than for a monovacancy [39–42]. This suggests that the size of each open space due to this defect is small, i.e., this defect can be regarded as a kind of point defect. CL analysis suggests it to be a C_i–O_i complex. These two defects created after RTA in an O_2-containing atmosphere (V_2 and the C_i–O_i complex) are known to form the defects in the band gap at E_c −0.4 eV and E_v +0.38 eV, respectively [43,44]. These levels are shallower than the V_4 level at E_c −0.54 eV or V_5 level at E_c −0.47 eV, that is, the capture cross-section of V_2 or C_i–O_i complex is lower than V_4 or V_5 [45]. This appears to explain the falling sheet resistance with increasing O_2 content in the annealing atmosphere. Taking all the results together, we conclude that the damage remaining after RTA is transformed from large vacancy-type of defects, such as V_4 or V_5, to small vacancy-type defects (V_2) and oxygen-related defects (C_i–O_i complex), in proportion to the O_2 content in the annealing atmosphere.

Table 1
The lifetime and intensities for the RTA-applied samples with different proportion of O_2 concentration in annealing atmosphere (0% and 30%). These values were obtained in the analysis of lifetime spectra of positrons measured using the pulsed monoenergetic positron beam. The incident positron energy was fixed at E = 1 keV.

O_2 concentration (%)	τ_1 (ps)	τ_2 (ps)	I_2 (%)
0	359 ± 1		
30	198 ± 1	320 ± 1	36 ± 4

4. Conclusions

We characterized residual damage in low-dose (10^{13} cm^{-2}) As implanted Si that had been subjected to high-temperature (1100 °C) RTA with various concentrations of O_2 in the annealing atmosphere. Analysis of the CL results successfully revealed the presence of residual damage when using a rapid thermal process as heat treatment. This residual damage was identified as vacancy-type defects, such as V_4 or V_5, distributed at the surface and down to a few tens of nanometers by analyzing the Doppler broadenings of positron annihilation spectra. Further analysis, including sheet resistance variation, indicates that these vacancy-type defects are transformed to other types of defects (specifically V_2 or C_i–O_i complex defects) when O_2 gas is introduced to the annealing chamber. All the defects were confirmed to be created by a non-equilibrium reaction during the extremely rapid cooling step in the annealing sequence. Their effects on device performance should be studied.

Acknowledgements

We would like to express our gratitude to Dr. R. Sugie and K. Inoue for performing the CL measurement. We would like to thank F. Kawase for preparing the samples and S. Yoshikawa for analyzing SIMS profiles. We are also grateful to K. Ito and E. Igaki for their support.

References

[1] J.W. Mayer, L. Eriksson, J.A. Davis, Ion Implantation in Semiconductors, Academic Press, New York, 1970.
[2] L.N. Large, R.W. Bicknell, J. Mater. Sci. 2 (1967) 589.
[3] W.K. Wu, J. Washburn, J. Appl. Phys. 45 (1974) 1085.
[4] L. Eriksson, J.A. Davies, J. Denhartog, J.W. Mayer, O.J. Marsh, R. Markarious, Appl. Phys. Lett. 10 (1967) 323.
[5] R.R. Hart, O.J. Marsh, Appl. Phys. Lett. 15 (1969) 206.
[6] E. Landi, S. Solmi, Solid-State Electron. 29 (1986) 1181.
[7] N.E.B. Cowern, G.F.A. Van de Walle, P.C. Zalm, D.E.W. Vandenhoudt, Appl. Phys. Lett. 65 (1994) 2981.
[8] K.L. Brower, F.L. Vook, J.A. Borders, Appl. Phys. Lett. 15 (1969) 208.
[9] D.F. Daly, K.A. Pickar, Appl. Phys. Lett. 15 (1969) 267.
[10] H.J. Stein, F.L. Vook, J.A. Borders, Appl. Phys. Lett. 15 (1969) 328.
[11] B.L. Crowder, R.S. Title, M.H. Brodsky, G.D. Pettit, Appl. Phys. Lett. 16 (1970) 205.
[12] J.R. Nooman, C.G. Kirkpatrick, B.G. Streetman, Rad. Effects 21 (1974) 225.
[13] C.G. Kirkpatrick, J.R. Nooman, B.G. Streetman, Rad. Effects 30 (1976) 97.
[14] J. Krynicki, J.C. Bourgoin, Appl. Phys. 18 (1979) 275.
[15] K.L. Wang, Appl. Phys. Lett. 36 (1979) 48.
[16] M. Tamura, Appl. Phys. Lett. 23 (1973) 651.
[17] K.S. Jones, S. Prussin, E.R. Weber, Appl. Phys. A 45 (1988) 1.
[18] A. Sagara, M. Hiraiwa, S. Shibata, R. Sugie, K. Yamada, AIP Proc. 1321 (2010) 225.

[19] B.G. Yacobi, D.B. Holt, Cathodoluminescence Microscopy of Inorganic Solids, Plenum, New York, 1990.
[20] C.M. Parish, P.E. Russell, Scanning cathodoluminescence microscopy, in: P. Hawkes (Ed.), Advances in Imaging and Electron Physics, Academic, New York, 2007 (vol. 147).
[21] R. Sugie, T. Mitani, M. Yoshikawa, Y. Iwata, R. Satoh, Jpn. J. Appl. Phys. 49 (2010) 04DP15.
[22] R. Sugie, K. Matsuda, T. Ajioka, M. Yoshikawa, T. Mizukoshi, K. Shibusawa, S. Yo, J. Appl. Phys. 100 (2006) 064504.
[23] V.N. Faifer, M.I. Current, T.M.H. Wong, V.V. Souchkov, J. Vac. Sci. Technol., B 24 (1) (2006) 414–420.
[24] M.J. Puska, R.M. Nieminen, Rev. Mod. Phys. 66 (1994) 841.
[25] A. van Veen, H. Schut, J. de Vries, R.A. Hakvoort, M.R. Ijpma, AIP Conf. Proc. 218 (1991) 171.
[26] R. Suzuki, T. Ohdaira, T. Mikado, Radiat. Phys. Chem. 58 (2000) 603.
[27] P. Kirkegaard, M. Eldrup, O.E. Mogenson, N.J. Pedersen, Comput. Phys. Commun. 23 (1981) 307.
[28] A. Uedono, K. Tsustui, S. Ishibashi, H. Watanabe, S. Kubota, Y. Nakagawa, B. Mizuno, T. Hattori, H. Iwai, Jpn. J. Appl. Phys. 49 (2010) 051301.
[29] A. Uedono, T. Mori, K. Morisawa, K. Murakami, T. Ohdaira, R. Suzuki, T. Mikado, T. Ishioka, M. Kitajima, S. Hishita, H. Haneda, I. Sakaguchi, J. Appl. Phys. 93 (2003) 3228.
[30] G. Davies, Phys. Rep. 176 (1989) 83.
[31] G. Davies, E.C. Lightowlers, Z.E. Ciechanowsta, J. Phys. C 20 (1987) 191.
[32] P.K. Giri, S. Coffa, E. Rimini, Appl, Phys. Lett. 78 (2001) 291.
[33] P.K. Giri, Semicond. Sci. Technol. 20 (2005) 638.
[34] J.M. Trombetta, G.D. Watkins, Appl. Phys. Lett. 51 (1987) 1103.
[35] L.I. Khirunenko, M.G. Sosnin, Yu.V. Pomozov, L.I. Murin, V.P. Markevich, A.R. Peaker, L.M. Almeida, J. Coutinho, V.J.B. Torres, Phys. Rev. B 78 (2008) 155203.
[36] G. Davies, A.S. Oates, R.C. Newman, R. Woolley, E.C. Lightowlers, M.J. Binns, J.C. Wilkes, J. Phys. C 19 (1986) 841.
[37] S.M. Sze, Semiconductor Devices: Physics and Technology, second ed., Wiley, New York, 2002.
[38] A.S. Grove, Physics and Technology of Semiconductor Device, Wiley, New York, 1967.
[39] R. Krause-Rehberg, H.S. Leipner, Positron Annihilation in Semiconductors, Springer-Verlag, Berlin, 1999.
[40] Saito, Oshiyama, Phys. Rev. B 53 (1996) 7810.
[41] M. Hakala, M.J. Puska, R.M. Nieminen, Phys. Rev. B 57 (1997) 7621.
[42] M.J. Puska, C. Corbel, Phys. Rev. B 38 (1988) 9874.
[43] G.D. Watkins, J.W. Corbett, Phys. Rev. 138 (1965) A543.
[44] P.M. Mooney, L.J. Cheng, M. Suli, J.D. Gerson, J.W. Corbett, Phys. Rev. B 15 (1977) 3836.
[45] P. Santos, J. Continho, M.J. Rayson, P.R. Briddon, Phys. Status Solidi C 9 (2012) 2000.